2013 American Control Conference (ACC)
Washington, DC, USA, June 17-19, 2013

Learning in the synthesis of data-driven variable-gain controllers

Marcel Heertjes, Bram Hunnekens, Nathan van de Wouw, and Henk Nijmeijer

***Abstract*— To deal with performance trade-offs in the control of motion systems, a method is developed for designing variable-gain feedback controllers. The idea is to select a piecewise affine controller structure and, subsequently, to find the nonlinear controller parameter values of this structure by data-driven performance optimization. Herein an $\mathcal{H}_2$ performance objective is minimized. As a result, variable-gain controllers are synthesized using techniques from the field of learning and optimization. The method is applied to a wafer stage simulation model.**

***Index Terms*— data-driven optimization, gradient methods, Lur'e systems, motion control, self-tuning, wafer scanners**

I. INTRODUCTION

In the wafer scanning industry [4] variable-gain control is used to deal with performance trade-offs otherwise occurring under linear feedback; see also [9], [12], [13], [20]. The rationale is that low-frequency vibrations induced by the motion set-points of wafer scanners are better suppressed under high-gain feedback. Contrarily, high-frequency noise encountered during constant (scanning) velocity, thus in the absence of said set-points, becomes less amplified under low-gain feedback. Exploiting the property of continuously varying the controller gain, for example by using a deadzone nonlinearity in the controller structure [6], variable-gain control provides the means to suppress set-point induced vibrations under high-gain feedback in one part of the scan while keeping a low-gain noise response in another part.

Tuning of the variable gain controller generally refers to frequency-domain loop shaping of the underlying linear system [6]. This is done by splitting up the nonlinear system into a linear system in feedback connection with a nonlinearity, i.e. adopt a Lur'e system formulation [21]. The linear system represents a closed-loop motion system, whose characteristics are the result of frequency-domain tunings [18]. On the one hand, these tunings should render the closed-loop system robustly stable, i.e. being able to deal with the effect of plant resonances (and the uncertainty thereabout) on the closed-loop stability properties. On the other hand, the tunings aim at improved closed-loop performance properties in view of the trade-off between low-frequency disturbance suppression and high-frequency noise amplification.

Stability of the nonlinear closed-loop system can be guaranteed by frequency-domain evaluation through the circle criterion [6]. Performance, however, very much depends on the choice of the variable gains, the plant characteristics, and the (unknown) disturbances acting on the system, which vary from machine to machine but also from field (wafer area during exposure) to field. It therefore makes sense to assess (servo) performance per machine or field and in time domain, the latter in view of the nonlinearity in the loop.

This paper explicitly deals with the performance-based design of the nonlinear part of the Lur'e system. Observing that an accurate model description of the plant and the disturbances (suited for performance evaluation) is often lacking, an early selection of a fixed nonlinear structure, e.g. deadzone or saturation [1], is not likely to induce best time-domain performances on individual machines during later machine qualifications. In [7], this problem was (only partly) tackled by self-tuning of the parameters of a deadzone nonlinearity, which was done per machine. With an iterative data-driven approach, see [2], [3], [5], [14] for other approaches, sampled data provided the information to find an updated set of parameters on the basis of least-squares optimization; for self-tuning in the nonlinear context, see also [8], [11], [16].

In this paper, the nonlinearity is given by piecewise affine functions having neither pre-defined gains nor switching lengths. Adopting the iterative approach from [7] gives a method for data-driven variable-gain controller synthesis in which the gains and switching lengths can be tuned per machine or even (in the learning sense) from field to field. The latter has strong similarities with learning approaches having varying learning gains and/or Q-filters [19]. In contrast with these approaches, however, the method presented here considers (nonlinear) filter design rather than signal design. Also, it classifies under feedback instead of under feedforward control. In a companion paper [10], a model-based approach is considered which is more suited for (large-scale) parameter studies conducted in the design phase when no machine measurements are yet available. Depending on the specific disturbances and plant characteristics, the nonlinearity can become deadzone, saturation, or any other structure the piecewise affine function supports; this is different from [7] where a fixed deadzone structure is used. Dedicated optimization of machine performance is obtained with guaranteed (robust) stability properties. This is favorable for the motion industry in dealing with performance variation among machines, and for the wafer scanning industry in particular.

The remainder of the paper is organized as follows. In Section 2, the Lur'e-type system description of the variable-gain motion control system is discussed. This includes the introduction of a three-parameter piecewise affine (variable-gain) function, a stability analysis using the circle criterion, and a lifted system description describing the closed-loop dynamics of a sampled-data implementation of the nonlinear controller. In Section 3, a data-driven $\mathcal{H}_2$ optimization approach is presented that is used to find the optimal parameters of the piecewise affine function. Section 4 addresses a generalization of the optimization method toward more arbitrary

All authors are with the Department of Mechanical Engineering, Eindhoven University of Technology, 5600 MB Eindhoven, The Netherlands. M.F. Heertjes is also with ASML, Veldhoven, The Netherlands. marcel.heertjes@asml.com This work is financially supported by the Dutch Technology Foundation STW.

978-1-4799-0176-0/$31.00 ©2013 AACC

piecewise affine functions. In Section 5, the optimization scheme is applied to a wafer stage model. In Section 5, the main conclusions and findings are summarized.

II. LUR'E SYSTEM DESCRIPTION

Consider the continuous-time Lur'e system:

$$\begin{aligned} \dot{x}(t) &= Ax(t) + b_1u(t) + b_2v(t) \\ y(t) &= c^{\mathrm{T}}x(t) + dv(t) \\ u(t) &= -\phi(y(t)), \end{aligned} \tag{1}$$

with state vector $x(t) \in \mathbb{R}^n$, input $u(t) \in \mathbb{R}$, output $y(t) \in \mathbb{R}$, $A \in \mathbb{R}^{n\times n}$ a Hurwitz matrix, matrices $b_1, b_2, c \in \mathbb{R}^n$, the pair $\{A, b_1\}$ controllable, the pair $\{A, c^{\mathrm{T}}\}$ observable, $v(t) \in \mathbb{R}$ a uniformly bounded disturbance: $\limsup_{t\to\infty} v(t) = \bar{v}$, and odd piecewise affine function $y(t) \mapsto \phi(y(t))$:

$$\phi(y(t)) = \phi_1(y(t))y(t) + \delta_1\phi_2(y(t)), \tag{2}$$

where

$$\phi_1(y(t)) = \begin{cases} \alpha_1, & \text{if } |y(t)| < \delta_1 \\ \tfrac{1}{2}(\alpha_1+\alpha_2), & \text{if } |y(t)| = \delta_1 \\ \alpha_2, & \text{if } |y(t)| > \delta_1 \end{cases}, \tag{3}$$

and

$$\phi_2(y(t)) = \begin{cases} 0, & \text{if } |y(t)| < \delta_1 \\ \tfrac{1}{2}(\alpha_1-\alpha_2)\mathrm{sign}(y(t)), & \text{if } |y(t)| = \delta_1 \\ (\alpha_1-\alpha_2)\mathrm{sign}(y(t)), & \text{if } |y(t)| > \delta_1 \end{cases}. \tag{4}$$

A graphical representation of (2) is given in Fig.1. For switching length δ_1 satisfying the bound $\delta_{\max} \geq \delta_1 \geq 0$ and gains $\alpha_i,\ i = 1, 2$, satisfying the bound $\alpha_{\max} \geq \alpha_1, \alpha_2 \geq 0$, it follows that $y(t)$,$u(t)$ in (1) satisfy the sector condition:

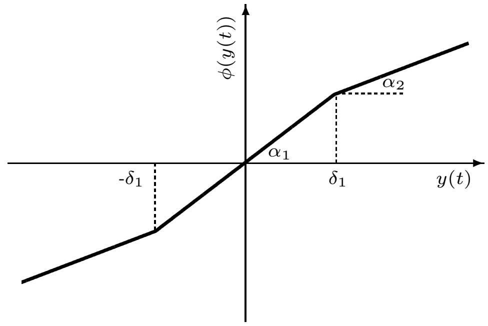

Fig. 1. Graphical representation of (2).

$$\alpha_{\max}u(t)y(t) \leq -u^2(t). \tag{5}$$

A motion control structure that fits the description in (1) is given in Fig. 2. In this figure, $\mathcal{C}$ represents a linear time-invariant controller, $\mathcal{P}$ represents the motion system itself, and $\phi(y)$ represents an additive variable (controller) gain as in (2). The frequency-domain relation between inputs $U(j\omega)$, $V(j\omega)$ and output $Y(j\omega)$ related to u, v, y, respectively, i.e. the linear part of the model in (1), reads:

$$Y(j\omega) = \mathcal{S}_c(j\omega)U(j\omega) + \mathcal{S}(j\omega)V(j\omega), \tag{6}$$

with the complementary sensitivity function $\mathcal{S}_c(j\omega) \in \mathbb{C}$ and the sensitivity function $\mathcal{S}(j\omega) \in \mathbb{C}$ defined by:

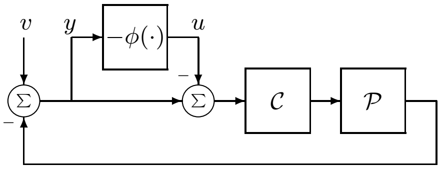

Fig. 2. Block diagram of a motion control system described by (1).

$$\begin{aligned} \mathcal{S}_c(j\omega) &= c^{\mathrm{T}}(j\omega I - A)^{-1}b_1 = \frac{\mathcal{P}(j\omega)\mathcal{C}(j\omega)}{1+\mathcal{P}(j\omega)\mathcal{C}(j\omega)}, \\ \mathcal{S}(j\omega) &= c^{\mathrm{T}}(j\omega I - A)^{-1}b_2 + d = \frac{1}{1+\mathcal{P}(j\omega)\mathcal{C}(j\omega)}. \end{aligned} \tag{7}$$

A sufficient condition for input-to-state stability of (1) follows from the circle criterion (see for example [21]) which, given (5), in the frequency-domain reads:

$$\Re\{\mathcal{S}_c(j\omega)\} \geq -\frac{1}{\alpha_{\max}}. \tag{8}$$

Stability thus follows from the linear system properties between input u and output y, which can be shaped for stability (to satisfy (8)) and for closed-loop performance using straightforward loop-shaping techniques [6].

In discrete-time, assume that (1) can be written as:

$$\begin{aligned} x(k+1) &= \hat{A}x(k) + \hat{b}_1u(k) + \hat{b}_2v(k) \\ y(k) &= \hat{c}^{\mathrm{T}}x(k) + \hat{d}v(k) \\ u(k) &= -\phi(y(k)), \end{aligned} \tag{9}$$

with state vector $x(k) \in \mathbb{R}^n$, $\hat{A} \in \mathbb{R}^{n\times n}$ Hurwitz, matrices $\hat{b}_1, \hat{b}_2, \hat{c} \in \mathbb{R}^n$, the pair $\{\hat{A}, \hat{b}_1\}$ controllable, the pair $\{\hat{A}, \hat{c}^{\mathrm{T}}\}$ observable, and $u(k), v(k), y(k) \in \mathbb{R}$ time-sampled signals at counter $k \in \mathbb{N}$; note that the aforementioned properties depend on the discretization scheme (and sampling interval) used. The linear part of system (9) can be put in lifted form:

$$\begin{bmatrix} y(1) \\ \vdots \\ y(k) \end{bmatrix} = \overbrace{\begin{bmatrix} 0 & & \cdots & 0 \\ \hat{c}^{\mathrm{T}}\hat{b}_1 & & & \vdots \\ \vdots & \ddots & \ddots & \\ \hat{c}^{\mathrm{T}}\hat{A}^{k-2}\hat{b}_1 & \cdots & \hat{c}^{\mathrm{T}}\hat{b}_1 & 0 \end{bmatrix}}^{\mathbf{S}_c} \begin{bmatrix} u(1) \\ \vdots \\ u(k) \end{bmatrix}$$

$$+ \underbrace{\begin{bmatrix} \hat{d} & 0 & \cdots & 0 \\ \hat{c}^{\mathrm{T}}\hat{b}_2 & & & \vdots \\ \vdots & \ddots & \ddots & 0 \\ \hat{c}^{\mathrm{T}}\hat{A}^{k-2}\hat{b}_2 & \cdots & \hat{c}^{\mathrm{T}}\hat{b}_2 & \hat{d} \end{bmatrix}}_{\mathbf{S}} \begin{bmatrix} v(1) \\ \vdots \\ v(k) \end{bmatrix} + \begin{bmatrix} \hat{c}^{\mathrm{T}} \\ \hat{c}^{\mathrm{T}}\hat{A} \\ \vdots \\ \hat{c}^{\mathrm{T}}\hat{A}^{k-1} \end{bmatrix} x(1), \tag{10}$$

with $\mathbf{y}_\kappa = [y(1)\ldots y(k)]^{\mathrm{T}}$, $\mathbf{u}_\kappa = [u(1)\ldots u(k)]^{\mathrm{T}}$, $\mathbf{v}_\kappa = [v(1)\ldots v(k)]^{\mathrm{T}}$, and $\kappa \in \mathbb{N}$ referring to a specific realization/iteration of the gathered data samples. Let

$$\varphi(\mathbf{y}_\kappa) = \varphi_1(\mathbf{y}_\kappa)\mathbf{y}_\kappa + \delta_1\varphi_2(\mathbf{y}_\kappa), \tag{11}$$

with diagonal matrix $\varphi_1(\mathbf{y}_\kappa)[i,i] = \phi_1(y(i))$, see (3), and

$\varphi_2(\mathbf{y}_\kappa)[i] = \phi_2(y(i))$, see (4). For $\mathbf{v}_\kappa(\kappa) = [v(1)\dots v(k)]^{\mathrm{T}}$, and $x(1) = 0$, it then follows that (9) can be represented in the following discretized and lifted form:

$$\mathbf{y}_\kappa = \mathbf{S}_c\mathbf{u}_\kappa + \mathbf{S}\mathbf{v}_\kappa \tag{12a}$$

$$\mathbf{u}_\kappa = -\varphi(\mathbf{y}_\kappa). \tag{12b}$$

The matrices $\mathbf{S}_c, \mathbf{S} \in \mathbb{R}^{k\times k}$ contain the impulse responses of the linear stable systems in (7): $\mathcal{S}_c, \mathcal{S}$, respectively. Eq.(12a) represents a discrete-time convolution from the input signals $\mathbf{u}_\kappa, \mathbf{v}_\kappa \in \mathbb{R}^k$ to the output signal $\mathbf{y}_\kappa \in \mathbb{R}^k$, see also (6).

For the system in (12) with $\varphi(\mathbf{y}_\kappa) \in \mathbb{R}^k$ in (11) the aim is to find values for $\delta_1, \alpha_1, \alpha_2$ that render desired closed-loop behavior. For this purpose, an iterative $\mathcal{H}_2$ optimization approach will be proposed.

III. $\mathcal{H}_2$ OPTIMIZATION APPROACH

Consider the $\mathcal{H}_2$ cost function:

$$J = \mathbf{y}_\kappa{}^{\mathrm{T}}\mathbf{y}_\kappa + \beta\mathbf{u}_\kappa{}^{\mathrm{T}}\mathbf{u}_\kappa, \tag{13}$$

which represents a weighted sum of quadratic forms for the inputs and outputs of the linear part of the Lur'e system in (12a) with weighting $\beta \geq 0$. Penalizing $\mathbf{y}_\kappa \in \mathbb{R}^k$ keeps a small error response, see Fig. 2. The reason to penalize $\mathbf{u}_\kappa \in \mathbb{R}^k$ is that any harmonic input $y(t) \in \mathbb{R}$ to $\phi(y(t)) \in \mathbb{R}$ in (1) potentially induces higher harmonics in the output $u(t) \in \mathbb{R}$ which, subsequently, may excite high-frequency dynamics of the controlled plant. The nonlinear operation can therefore be seen as a generator of noise which through β in (13) gets penalized.

Let the parameter vector to-be-optimized be defined by:

$$\mathbf{p}(\kappa) = \begin{bmatrix}\delta_1(\kappa) & \alpha_1(\kappa) & \alpha_2(\kappa)\end{bmatrix}^{\mathrm{T}}. \tag{14}$$

With the Gauss-Newton method, which is widely used for minimization of a sum of squared function values [3], $\mathbf{p}(\kappa) \in \mathbb{R}^3$ that minimizes (13), or:

$$\tilde{\mathbf{p}} = \arg\min_{\mathbf{p}(\kappa)} J, \tag{15}$$

is found through:

$$\begin{aligned}\mathbf{p}(\kappa+1) = \mathbf{p}(\kappa) - \zeta(\nabla^{\mathrm{T}}\mathbf{y}_\kappa\nabla\mathbf{y}_\kappa + \beta\nabla^{\mathrm{T}}\mathbf{u}_\kappa\nabla\mathbf{u}_\kappa)^{-1}\\ \times(\nabla^{\mathrm{T}}\mathbf{y}_\kappa\mathbf{y}_\kappa + \beta\nabla^{\mathrm{T}}\mathbf{u}_\kappa\mathbf{u}_\kappa),\end{aligned} \tag{16}$$

with damping coefficient $0 < \zeta \leq 1$ and gradients:

$$\begin{aligned}\nabla\mathbf{y}_\kappa &= \begin{bmatrix}\frac{\partial\mathbf{y}_\kappa}{\partial\delta_1} & \frac{\partial\mathbf{y}_\kappa}{\partial\alpha_1} & \frac{\partial\mathbf{y}_\kappa}{\partial\alpha_2}\end{bmatrix} \text{ and}\\ \nabla\mathbf{u}_\kappa &= \begin{bmatrix}\frac{\partial\mathbf{u}_\kappa}{\partial\delta_1} & \frac{\partial\mathbf{u}_\kappa}{\partial\alpha_1} & \frac{\partial\mathbf{u}_\kappa}{\partial\alpha_2}\end{bmatrix}.\end{aligned} \tag{17}$$

Using (10) and (11), it follows (after some algebra) that:

$$\begin{aligned}\frac{\partial\mathbf{y}_\kappa}{\partial\delta_1} &= \mathbf{S}_c\frac{\partial\mathbf{u}_\kappa}{\partial\delta_1} = -\mathbf{S}_c\frac{\partial\varphi(\mathbf{y}_\kappa)}{\partial\delta_1}\\ &= -\mathbf{S}_c\left(\varphi_1(\mathbf{y}_\kappa)\frac{\partial\mathbf{y}_\kappa}{\partial\delta_1} + \varphi_2(\mathbf{y}_\kappa)\right).\end{aligned} \tag{18}$$

This subsequently leads to:

$$\frac{\partial\mathbf{y}_\kappa}{\partial\delta_1} = -\mathbf{A}(\mathbf{y}_\kappa)\varphi_2(\mathbf{y}_\kappa),\ \frac{\partial\mathbf{u}_\kappa}{\partial\delta_1} = -\mathbf{A}^*(\mathbf{y}_\kappa)\varphi_2(\mathbf{y}_\kappa), \tag{19}$$

with $\mathbf{A}(\mathbf{y}_\kappa) = (\mathbf{I} + \mathbf{S}_c\varphi_1(\mathbf{y}_\kappa))^{-1}\mathbf{S}_c \in \mathbb{R}^{k\times k}$ and $\mathbf{A}^*(\mathbf{y}_\kappa) = (\mathbf{I} + \varphi_1(\mathbf{y}_\kappa)\mathbf{S}_c)^{-1} \in \mathbb{R}^{k\times k}$. Similarly, it can be checked that:

$$\begin{aligned}\frac{\partial\mathbf{y}_\kappa}{\partial\alpha_1} &= -\mathbf{A}(\mathbf{y}_\kappa)\mathrm{sat}(\mathbf{y}_\kappa),\\ \frac{\partial\mathbf{y}_\kappa}{\partial\alpha_2} &= -\mathbf{A}(\mathbf{y}_\kappa)(\mathbf{y}_\kappa - \mathrm{sat}(\mathbf{y}_\kappa))\\ &= -\mathbf{A}(\mathbf{y}_\kappa)\mathbf{y}_\kappa - \frac{\partial\mathbf{y}_\kappa}{\partial\alpha_1},\end{aligned} \tag{20}$$

with $\mathrm{sat}(\mathbf{y}_\kappa) = [\mathrm{sat}(y(1))\dots\mathrm{sat}(y(k))]^{\mathrm{T}} \in \mathbb{R}^k$, $y(i) \mapsto \mathrm{sat}(y(i))$ with $i \in \{1,\dots,k\}$ according to:

$$\mathrm{sat}(y(i)) = \begin{cases}y(i), & \text{if } |y(i)| \leq \delta_1\\ \delta_1\mathrm{sign}(y(i)), & \text{otherwise,}\end{cases} \tag{21}$$

and

$$\begin{aligned}\frac{\partial\mathbf{u}_\kappa}{\partial\alpha_1} &= -\mathbf{A}^*(\mathbf{y}_\kappa)\mathrm{sat}(\mathbf{y}_\kappa),\\ \frac{\partial\mathbf{u}_\kappa}{\partial\alpha_2} &= -\mathbf{A}^*(\mathbf{y}_\kappa)\mathbf{y}_\kappa - \frac{\partial\mathbf{u}_\kappa}{\partial\alpha_1}.\end{aligned} \tag{22}$$

In deriving the gradient error signals in (18) and (19), we explicitly use the fact that:

$$\frac{\partial\phi_1(y(t))}{\partial y(t)}y(t) + \frac{\partial\phi_2(y(t))}{\partial y(t)}\delta_1 = 0, \tag{23a}$$

$$\frac{\partial\phi_1(y(t))}{\partial\delta_1}y(t) + \frac{\partial\phi_2(y(t))}{\partial\delta_1}\delta_1 = 0. \tag{23b}$$

This follows from writing $\phi_1(y(t)), \phi_2(y(t)) \in \mathbb{R}$ in (3) and (4) as:

$$\begin{aligned}\phi_1(y(t)) &= \lim_{z\to 0}\left\{\alpha_1 - \left(\frac{\alpha_2-\alpha_1}{\pi}\arctan\left(\frac{2\pi(y(t)+\delta_1)}{z}\right)\right.\right.\\ &\qquad\left.\left. - \frac{\alpha_2-\alpha_1}{\pi}\arctan\left(\frac{2\pi(y(t)-\delta_1)}{z}\right)\right)\right\},\\ \phi_2(y(t)) &= \lim_{z\to 0}\left\{-\frac{\alpha_2-\alpha_1}{\pi}\arctan\left(\frac{2\pi(y(t)+\delta_1)}{z}\right)\right.\\ &\qquad\left. - \frac{\alpha_2-\alpha_1}{\pi}\arctan\left(\frac{2\pi(y(t)-\delta_1)}{z}\right)\right\},\end{aligned} \tag{24}$$

with input $y(t) \in \mathbb{R}$ and switching length $\delta_1 > 0$. The partial derivatives read:

$$\begin{aligned}\frac{\partial\phi_1(y(t))}{\partial y(t)} &= \lim_{z\to 0}\left\{-\frac{2(\alpha_2-\alpha_1)z}{z^2+4\pi^2(y(t)+\delta_1)^2}\right.\\ &\qquad\left. + \frac{2(\alpha_2-\alpha_1)z}{z^2+4\pi^2(y(t)-\delta_1)^2}\right\}\\ \frac{\partial\phi_2(y(t))}{\partial y(t)} &= \lim_{z\to 0}\left\{-\frac{2(\alpha_2-\alpha_1)z}{z^2+4\pi^2(y(t)+\delta_1)^2}\right.\\ &\qquad\left. - \frac{2(\alpha_2-\alpha_1)z}{z^2+4\pi^2(y(t)-\delta_1)^2}\right\},\end{aligned} \tag{25}$$

which only for $y(t) = \delta_1$ and $y(t) = -\delta_1$ are non-zero valued. Let $y(t) = \delta_1$, it then follows that:

$$\begin{aligned}&\frac{\partial \phi_1(y(t))}{\partial y(t)}\delta_1 + \frac{\partial \phi_2(y(t))}{\partial y(t)}\delta_1 \\ &= \lim_{z\to 0}\left\{-\frac{2(\alpha_2-\alpha_1)\delta_1 z}{z^2+16\pi^2\delta_1^2} + \frac{2(\alpha_2-\alpha_1)\delta_1 z}{z^2}\right. \\ &\qquad \left. -\frac{2(\alpha_2-\alpha_1)\delta_1 z}{z^2+16\pi^2\delta_1^2} - \frac{2(\alpha_2-\alpha_1)\delta_1 z}{z^2}\right\} \\ &= \lim_{z\to 0}\left\{-\frac{4(\alpha_2-\alpha_1)\delta_1 z}{z^2+16\pi^2\delta_1^2}\right\} = 0.\end{aligned} \tag{26}$$

The same holds true for $y(t) = -\delta_1$, hence the validity of (23a); (23b) follows from similar reasonings.

IV. EXTENSIONS

Consider the straightforward extension of (2) toward $m > 2$ gains and $m-1$ switching lengths. For $\alpha_{\text{max}} \geq \alpha_1, \alpha_2 \ldots \alpha_m \geq 0$ and $\delta_{\text{max}} \geq \delta_{m-1} \geq \cdots \geq \delta_1 \geq 0$, $\phi(y) \in \mathbb{R}$ (where $y(t) \mapsto \phi(y(t))$) reads:

$$\begin{aligned}\phi(y(t)) = \phi_1(y(t))y(t) + \delta_1\phi_{2,1}(y(t)) + \\ \cdots + \delta_{m-1}\phi_{2,m-1}(y(t)),\end{aligned} \tag{27}$$

where $y(t) \mapsto \phi_1(y(t))$:

$$\phi_1(y(t)) = \begin{cases}\alpha_1, & \text{if } |y(t)| < \delta_1 \\ ½(\alpha_1-\alpha_2), & \text{if } |y(t)| = \delta_1 \\ \alpha_2, & \text{if } \delta_1 < |y(t)| < \delta_2 \\ \vdots & \\ \alpha_{m-1}, & \text{if } \delta_{m-2} < |y(t)| < \delta_{m-1} \\ ½(\alpha_{m-1}-\alpha_m), & \text{if } |y(t)| = \delta_{m-1} \\ \alpha_m, & \text{if } |y(t)| > \delta_{m-1}\end{cases}, \tag{28}$$

with $y \mapsto \phi_{2,j}(y(t))$ and $j \in \{1, \ldots, m-1\}$:

$$\phi_{2,j}(y(t)) = \begin{cases}0, & \text{if } |y(t)| < \delta_j \\ ½(\alpha_j-\alpha_{j+1})\text{sign}(y(t)), & \text{if } |y(t)| = \delta_j \\ (\alpha_j-\alpha_{j+1})\text{sign}(y(t)), & \text{if } |y(t)| > \delta_j\end{cases}. \tag{29}$$

A graphical representation of (27) is given in Fig. 3. Since both (2) and (27) satisfy the sector condition in (5), closed-loop (robust) stability follows from repeating earlier arguments. In optimizing the parameters using the cost function $J \in \mathbb{R}$ in (13), the parameter vector $\mathbf{p}(\kappa) \in \mathbb{R}^{2m-1}$ becomes:

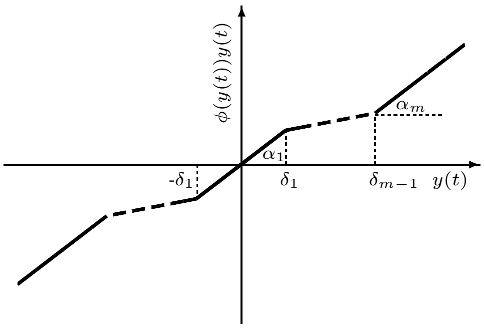

Fig. 3. Graphical representation of (27).

$$\mathbf{p}(\kappa) = \left[\delta_1(\kappa)\ldots\delta_{m-1}(\kappa) \quad \alpha_1(\kappa)\ldots\alpha_m(\kappa)\right]^{\text{T}}, \tag{30}$$

whereas in (16) the following gradients are used:

$$\begin{aligned}\nabla\mathbf{y}_\kappa &= \left[\frac{\partial\mathbf{y}_\kappa}{\partial\delta_1}\cdots\frac{\partial\mathbf{y}_\kappa}{\partial\delta_{m-1}} \quad \frac{\partial\mathbf{y}_\kappa}{\partial\alpha_1}\cdots\frac{\partial\mathbf{y}_\kappa}{\partial\alpha_m}\right] \text{ and} \\ \nabla\mathbf{u}_\kappa &= \left[\frac{\partial\mathbf{u}_\kappa}{\partial\delta_1}\cdots\frac{\partial\mathbf{u}_\kappa}{\partial\delta_{m-1}} \quad \frac{\partial\mathbf{u}_\kappa}{\partial\alpha_1}\cdots\frac{\partial\mathbf{u}_\kappa}{\partial\alpha_m}\right].\end{aligned} \tag{31}$$

By redefining $\varphi(\mathbf{y}_\kappa) = \varphi_1(\mathbf{y}_\kappa)\mathbf{y}_\kappa + \delta_1\varphi_{2,1}(\mathbf{y}_\kappa) + \cdots + \delta_{m-1}\varphi_{2,m-1}(\mathbf{y}_\kappa) \in \mathbb{R}^{k\times k}$, with $\varphi_1(\mathbf{y}_\kappa)[i,i] = \phi_1(y(i)) \in \mathbb{R}$ from (28) and $\varphi_{2,j}(\mathbf{y}_\kappa)[i] = \phi_2(y(i)) \in \mathbb{R}$ from (29) where $i \in \{1, \ldots, k\}$, $j \in \{1 \ldots m-1\}$, it follows using (18) that:

$$\frac{\partial\mathbf{y}_\kappa}{\partial\delta_j} = -\mathbf{A}(\mathbf{y}_\kappa)\varphi_{2,j}(\mathbf{y}_\kappa), \frac{\partial\mathbf{u}_\kappa}{\partial\delta_j} = -\mathbf{A}^*(\mathbf{y}_\kappa)\varphi_{2,j}(\mathbf{y}_\kappa). \tag{32}$$

Define $\text{sat}_j(\mathbf{y}_\kappa) = [\text{sat}_j(y(1))\ldots\text{sat}_j(y(k))]^{\text{T}} \in \mathbb{R}^k$, with

$$\text{sat}_j(y(i)) = \begin{cases}y(i), & \text{if } |y(i)| \leq \delta_j \\ \delta_j\text{sign}(y(i)), & \text{otherwise,}\end{cases} \tag{33}$$

it then follows for $j \in \{2 \ldots m-1\}$ that:

$$\begin{aligned}\frac{\partial\mathbf{y}_\kappa}{\partial\alpha_1} &= -\mathbf{A}(\mathbf{y}_\kappa)\text{sat}_1(\mathbf{y}_\kappa), \\ \frac{\partial\mathbf{y}_\kappa}{\partial\alpha_j} &= -\mathbf{A}(\mathbf{y}_\kappa)(\text{sat}_j(\mathbf{y}_\kappa) - \text{sat}_{j-1}(\mathbf{y}_\kappa)), \\ \frac{\partial\mathbf{y}_\kappa}{\partial\alpha_m} &= -\mathbf{A}(\mathbf{y}_\kappa)(\mathbf{y}_\kappa - \text{sat}_{m-1}(\mathbf{y}_\kappa)), \\ \frac{\partial\mathbf{u}_\kappa}{\partial\alpha_1} &= -\mathbf{A}^*(\mathbf{y}_\kappa)\text{sat}_1(\mathbf{y}_\kappa), \\ \frac{\partial\mathbf{u}_\kappa}{\partial\alpha_j} &= -\mathbf{A}^*(\mathbf{y}_\kappa)(\text{sat}_j(\mathbf{y}_\kappa) - \text{sat}_{j-1}(\mathbf{y}_\kappa)), \\ \frac{\partial\mathbf{u}_\kappa}{\partial\alpha_m} &= -\mathbf{A}^*(\mathbf{y}_\kappa)(\mathbf{y}_\kappa - \text{sat}_{m-1}(\mathbf{y}_\kappa)).\end{aligned} \tag{34}$$

V. WAFER STAGE EXAMPLE

By means of example, consider system (9) with:

$$\begin{aligned}&\hat{A} = \\ &\begin{bmatrix}4.26 & -2.0582 & 1.20476 & -0.9063 & 0.39955 & -0.30618 \\ 4 & 0 & 0 & 0 & 0 & 0 \\ 0 & 2 & 0 & 0 & 0 & 0 \\ 0 & 0 & 1 & 0 & 0 & 0 \\ 0 & 0 & 0 & 1 & 0 & 0 \\ 0 & 0 & 0 & 0 & 0.25 & 0\end{bmatrix}, \\ &\hat{b}_1 = -\hat{b}_2 = \begin{bmatrix}0.1250 \\ 0 \\ 0 \\ 0 \\ 0 \\ 0\end{bmatrix}, \hat{c} = \begin{bmatrix}0.1025 \\ 0.0305 \\ -0.0206 \\ -0.0253 \\ 0.0083 \\ 0.0419\end{bmatrix}, \hat{d} = 1,\end{aligned} \tag{35}$$

and the nonlinearity described in (2). System (9) satisfies the conditions imposed by the circle criterion with $\alpha_{\text{max}} = 0.5$. It describes a fourth-order wafer stage model that is controlled in discrete-time (with sampling time $T_s = 200$ μseconds) by a proportional-integral-derivative (PID) controller and additional first-order low-pass filter, see also [7]. The state vector $x(k) \in \mathbb{R}^6$ has four states coming from the fourth-order plant model, one coming from the PID controller, and one coming from the low-pass filter.

In (9), the input signal $v(k) \in \mathbb{R}$ is chosen as:

$$\begin{aligned} v(k) = \; & v_1\psi(kT_s)(\sin(2\pi 100kT_s) + \sin(2\pi 375kT_s)) \\ & + v_2\psi(kT_s - \tau)\sin(2\pi 375kT_s), \end{aligned} \tag{36}$$

with $v_1 = 30$ nm, $v_2 = 8$ nm, $\tau = 0.025$ s a scanning time constant, and Hanning function $kT_s \mapsto \psi(kT_s)$,

$$\psi(kT_s) = \begin{cases} 1 - \cos^2\left(\dfrac{\pi kT_s}{\tau}\right), & \text{if } 0 \leq kT_s \leq \tau \\ 0, \text{ otherwise.} \end{cases} \tag{37}$$

A distinction is made between two time intervals: $\tau_1 \in [0, \tau)$ and $\tau_2 \in [\tau, 2\tau]$. In the interval τ_1 a combination excitation is applied of a low-frequency disturbance (that can be suppressed by control) and a high-frequency disturbance that can only be amplified by said control. In the interval τ_2 merely the high-frequency disturbance is present, i.e. extra control can best be switched off. The input $v(k) \in \mathbb{R}$ is considered representative for a wafer scanning system where prior to scanning low-frequency set-point-induced vibrations dominate the error response whereas during scanning only high-frequency disturbances remain in effect [4], [6].

Prior to optimization, a brute-force simulation is conducted in which 8000 ($= 20^3$) time-series are processed for each of the 20 equally distributed parameter values considered for $\delta_1 \in \mathbb{R}$ and $\alpha_1, \alpha_2 \in \mathbb{R}$ and any combination thereof. For $\delta_1 \in \mathbb{R}$ these values are logarithmically spaced between 0.1 and 15 nanometer. For $\alpha_1, \alpha_2 \in \mathbb{R}$, this is done with a linear spacing in between the values of 0 and 2. Note that the circle criterion guarantees stability for $\alpha_1, \alpha_2 \leq 0.5$ which here seems rather conservative: linear reasoning (though strictly speaking not valid) indicates that a gain margin of 13.2 dB justifies a gain increase of 4.6! For $\beta = 0.05$, an evaluation of $J \in \mathbb{R}$ in (13) is shown in Fig. 4. The evaluation applies to the fixed value $\delta_1 =$ 11.52 nanometer which is the value found at the minimum $J = 1.6076\ 10^{-14}$ m^2 of all considered combinations. The optimum is found at $\alpha_1 = 0.2105$ and $\alpha_2 = 1.6842$; see the black dot in Fig. 4.

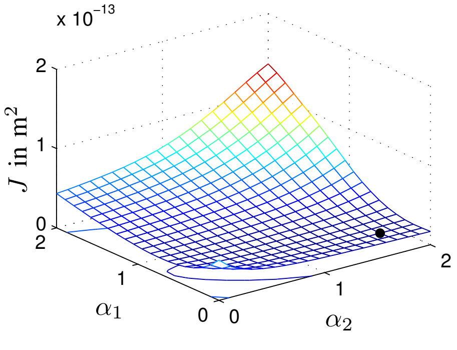

Fig. 4. Cost function evaluation after brute-force simulation for a cross-section with $\delta_1 = 11.52$ nm; the dimension of $\mathbf{y}_\kappa$ and $\mathbf{u}_\kappa$ in J is $k = 250$.

Returning to the optimization scheme[1] in (16), where the damping factor[2] is chosen at $\zeta = 0.5$, convergence of $J \in \mathbb{R}$ in (13) for two sets of initial conditions for the parameters is shown in Fig. 5. It can be seen that within $\kappa = 10$ iterations both sets converge to $J = 1.6044\,10^{-14}$ m^2, i.e. a value close (but somewhat smaller) to the value obtained with brute-force simulation; apparently the minimum is excluded from the analysis in Fig. 4 due to the considered equidistant parameter grid. Fig. 6 also shows that the parameters converge to $\delta_1 = 11.54$ nm, $\alpha_1 = 0.1736$, and $\alpha_2 = 1.7988$[3]. By replacing the time series obtained from simulation by time series obtained from measurement, the method is (in principle) directly applicable to sampled measurements.

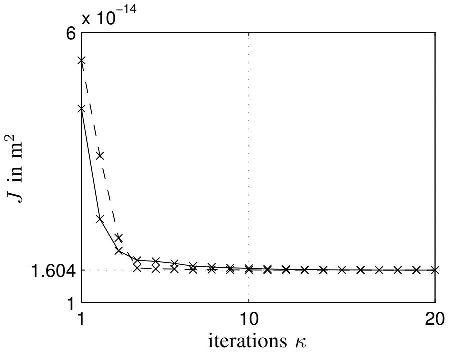

Fig. 5. Cost function evaluation during optimization with two sets of initial conditions for the parameters: set1 (low-gain) with $\{\delta_1, \alpha_1, \alpha_2\} = \{2\text{nm}, 0.01, 0.02\}$ and set2 (high-gain) with $\{\delta_1, \alpha_1, \alpha_2\} = \{1\text{nm}, 1.4, 1.5\}$.

Convergence of the structure of the nonlinearity along the iterations κ is considered in Fig. 7. The optimization renders a deadzone-like nonlinearity (thick black curve).

The effect of the optimization in terms of time-series simulation is shown in Fig. 8. For the input signal $v(k) \in \mathbb{R}$ in (36), it is clear that the optimized nonlinear structure gives no amplification of the high-frequency disturbance in the output (error) signal $y(k) \in \mathbb{R}$ in the second interval $\tau_2 \in [0.025, 0.05]$ seconds; the peak values are 12.1 nm. This is different from the initial high-gain settings (dashed gray curves) with peak values of 20.9 nm but similar to the

[1] In the simulations, a constrained optimization is conducted where $\epsilon_1 < \delta_1 \leq \delta_{\text{max}} = 20$ nm and $\epsilon_2 \leq \alpha_1, \alpha_2 \leq \alpha_{\text{max}} = 2$ with small positive constants: $\epsilon_1 = 10^{-2}$ nm and $\epsilon_2 = 10^{-2}$. As a result, the gradients in (17) do not become zero, which avoids the occurrence of trivial minima.

[2] Since the optimization problem is clearly non-convex, i.e. large values for δ_1 result in flattening of the cost function J, the convergence rate is kept smaller ($\zeta = 0.5$) than the rate induced by the system properties.

[3] In the example, $\delta_1 \in \mathbb{R}$ lies in the nanometer scale whereas $\alpha_1, \alpha_2 \in \mathbb{R}$ are in the order of 1. The scaling difference of 10^9 hampers the numerical computation of the inverse of the (approximated) Hessian $\tilde{\mathbf{H}} = \nabla^{\mathrm{T}}\mathbf{y}_\kappa\nabla\mathbf{y}_\kappa + \beta\nabla^{\mathrm{T}}\mathbf{u}_\kappa\nabla\mathbf{u}_\kappa \in \mathbb{R}^{3\times 3}$ in (16). As a solution to the problem, let $\mathbf{D} \in \mathbb{R}^{3\times 3}$ be a diagonal (scaling) matrix with scaling factors $\text{diag}(\mathbf{D}) = [10^9, 1, 1]$. Define the matrix $\tilde{\mathbf{H}}^* = \mathbf{D}\tilde{\mathbf{H}}\mathbf{D} \in \mathbb{R}^{3\times 3}$ which satisfies $\tilde{\mathbf{H}}^{-1} = \mathbf{D}(\tilde{\mathbf{H}}^*)^{-1}\mathbf{D} \in \mathbb{R}^{3\times 3}$. The inverse $\tilde{\mathbf{H}}^{-1} \in \mathbb{R}^{3\times 3}$ can thus be computed via the inverse of $\tilde{\mathbf{H}}^* \in \mathbb{R}^{3\times 3}$ which has all entries scaled in the same order of magnitude. Alternatively, $\delta_1 \in \mathbb{R}$, on the one hand, and $\alpha_1, \alpha_2 \in \mathbb{R}$, on the other hand, can be updated sequentially. First, $\delta_1 \in \mathbb{R}$ is updated under fixed values for $\alpha_1, \alpha_2 \in \mathbb{R}$, and, second, $\alpha_1, \alpha_2 \in \mathbb{R}$ are updated based on the (previously) updated value for $\delta_1 \in \mathbb{R}$. The last solution appeared the most successful and therefore was used.

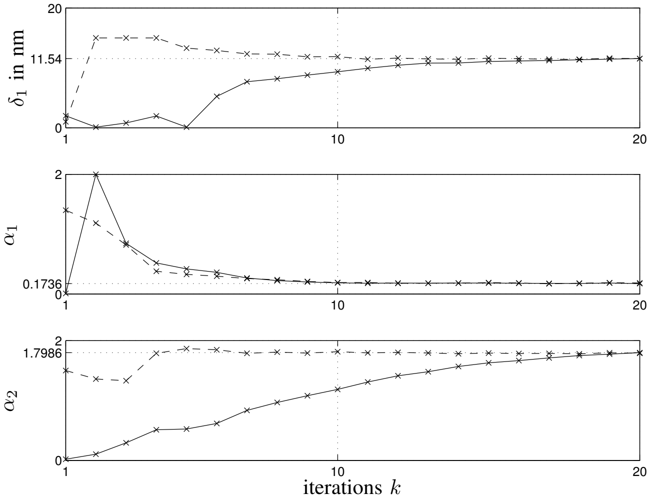

Fig. 6. Parameter convergence for two sets of initial conditions: set1 with $\{\delta_1, \alpha_1, \alpha_2\} = \{2\text{nm}, 0.01, 0.02\}$ and set2 with $\{\delta_1, \alpha_1, \alpha_2\} = \{1\text{nm}, 1.4, 1.5\}$.

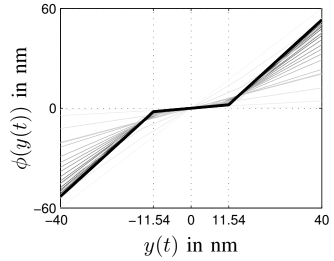

Fig. 7. Convergence of the structure of the nonlinearity along the iterations from $\kappa = 1$ (light gray) to $\kappa = 20$ (black) and for two sets of initial conditions.

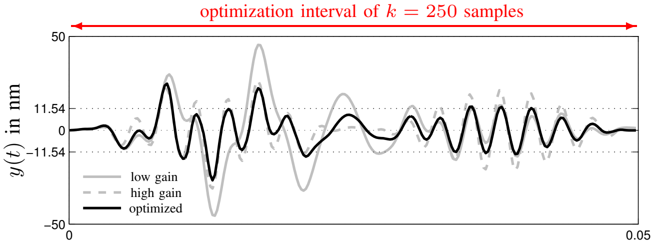

Fig. 8. Time-series simulation of the results after optimization, the low-gain settings with $\{\delta_1, \alpha_1, \alpha_2\} = \{0, 0, 0\}$, and a high-gain settings with $\{\delta_1, \alpha_1, \alpha_2\} = \{0, 0, 1\}$ in the optimization interval $t \in [0, 0.05]$.

initial low-gain settings (solid gray curves) with peak values of 14.32 nm. In the first interval $\tau_1 \in [0, 0.025)$ seconds the optimized structure induces a reduction of the low-frequency disturbance component with respect to the low-gain settings (the peak values reduce from 45.7 nm to 25.9 nm) and similar to the high gain settings with peak values of 27.8 nm. The optimized settings clearly yield improved performance. Note that improved performance is obtained by loosening the stability conditions set by the circle criterion which (in this case) appear overly conservative.

VI. Conclusions

By optimizing the structure of a nonlinear (variable-gain) feedback controller using a data-driven $\mathcal{H}_2$ approach, optimized machine performance can be obtained that remains inaccessible to any linear feedback controller. In the sense of a machine calibration, this has potential for motion control systems (in particular wafer stages) that exhibit a certain degree of repetitiveness, for example caused by recurring set-point motion and/or disturbances. If set-point motion varies from field to field, we envision an adaptive machine feedback which installs the process of iteratively learning the piecewise affine controller parameters, i.e. the structure of the nonlinearity.

References

[1] Armstrong BSR, Gutierrez JA, Wade BA, and Joseph R. (2006) Stability of phase-based gain modulation with designer-chosen switch functions. International Journal of Robotics Research, 25(8):781-796.

[2] Barton K and Alleyne A. (2008) A cross-coupled iterative learning control design for precision motion control. Transactions on Control Systems Technology, 16(6): 1218-1231.

[3] Bazanella AS, Campestrini L, and Eckhard D. (2012) Data-driven controller design; the $\mathcal{H}_2$ approach. Springer, New York.

[4] Butler H. (2011) Position control in lithographic equipment; an enabler for current-day chip manufacturing. IEEE Control Systems Magazine, 11:28-47.

[5] Hjalmarsson H. (2002) Iterative feedback tuning - an overview. International Journal of Adaptive Control and Signal Processing, 16: 373-395.

[6] Heertjes MF, Schuurbiers XGP, and Nijmeijer H. (2009) Performance improved design of N-PID controlled motion systems with application to wafer stages. Transactions on Industrial Electronics, 56(5):1347-1355.

[7] Heertjes MF and Nijmeijer H. (2012) Self-tuning of a switching controller for scanning motion systems. Mechatronics, 22:310-319.

[8] Hung L-C, Lin H-P, and Chung H-Y. (2007) Design of self-tuning fuzzy sliding mode control for TORA system. Expert Systems with Applications, 32:201-212.

[9] Hunnekens BGB, Van de Wouw N, and Nijmeijer H. (2012) Variable gain motion control for transient performance improvement. In Proc. American Control Conference, Montréal, Canada: 2467-2472.

[10] Hunnekens BGB, Heertjes MF, Van de Wouw N, and Nijmeijer H. (2013) Model-based piecewise affine variable-gain controller synthesis. In Proc. American Control Conference, Washington, WA, USA.

[11] Kuo TC, Huang YJ, and Chang SH. (2007) Sliding mode control with self-tuning law for uncertain nonlinear systems. ISA Transactions, 47:171-178.

[12] Lau K and Middleton RH. (2003) Switched integrator control schemes for integrating plants. European Journal of Control, 9(6):539-559.

[13] Lin Z, Pachter M, and Ban S. (1998) Toward improvement of tracking performance - nonlinear feedback for linear systems. International Journal of Control, 70(1):1-11.

[14] Mishra S, Yeh W, and Tomizuka M. (2008) Iterative learning control design for synchronization of wafer and reticle stages, In Proc. American Control Conference, Seattle, WA, USA: 3908-3913.

[15] Nešić D, Zaccarian L, and Teel AR. (2008) Stability properties of reset systems. Automatica, 44:2019-2026.

[16] Patete A, Furuta K, and Tomizuka M. (2008) Self-tuning control based on generalized minimum variance criterion for auto-regressive models. Automatica, 44:1970-1975.

[17] Scharuz SM and Schwartz AL. (1994) Design and optimal tuning of nonlinear PI compensators. Journal of Optimization Theory and Applications, 83:181-198.

[18] Steinbuch M and Norg ML. (1998) Advanced motion control: an industrial perspective. European Journal of Control, 4: 278-293.

[19] Tharayil M and Alleyne A. (2004) A time-varying iterative learning control scheme, In Proc. American Control Conference, Boston, MA, USA: 3782-3787.

[20] Van de Wouw N, Pastink E, Heertjes MF, Pavlov AV, and Nijmeijer H. (2008) Performance of convergence-based variable-gain control of optical storage drives. Automatica, 44(1): 15-27.

[21] Yakubovich VA, Leonov DA, and Gelig AKh. (2004) Stability of stationary sets in control systems with discontinuous nonlinearities. World Scientific, Singapore.